JACS
JOURNAL OF THE AMERICAN CHEMICAL SOCIETY
Article
pubs.acs.org/JACS

Gas-Phase Folding of a Prototypical Protonated Pentapeptide: Spectroscopic Evidence for Formation of a Charge-Stabilized β-Hairpin

Nicole L. Burke,[†] Andrew F. DeBlase, James G. Redwine,[‡] John R. Hopkins, Scott A. McLuckey,* and Timothy S. Zwier*

Department of Chemistry, Purdue University, West Lafayette, Indiana 47907-2084, United States

Supporting Information

ABSTRACT: Ultraviolet and infrared-ultraviolet (IR-UV) double-resonance photofragment spectroscopy has been carried out in a tandem mass spectrometer to determine the three-dimensional structure of cryogenically cooled protonated C-terminally methyl esterified leucine enkephalin $[YGGFL\text{-}OMe+H]^+$. By comparing the experimental IR spectrum of the dominant conformer with the predictions of DFT M05-2X/6-31+G(d) calculations, a backbone structure was assigned that is analogous to that previously assigned by our group for the unmodified peptide [Burke, N.L.; et al. *Int. J. Mass Spectrom.* **2015**, *378*, 196], despite the loss of a C-terminal OH binding site that was thought to play an important role in its stabilization. Both structures are characterized by a type II′ β-turn around Gly^3-Phe^4 and a γ-turn around Gly^2, providing spectroscopic evidence for the formation of a β-hairpin hydrogen bonding pattern. Rather than disrupting the peptide backbone structure, the protonated N-terminus serves to stabilize the β-hairpin by positioning itself in a pocket above the turn where it can form H-bonds to the Gly^3 and C-terminus C═O groups. This β-hairpin type structure has been previously proposed as the biologically active conformation of leucine enkephalin and its methyl ester in the nonpolar cell membrane environment [Naito, A.; Nishimura, K. *Curr. Top. Med. Chem.* **2004**, *4*, 135−143].

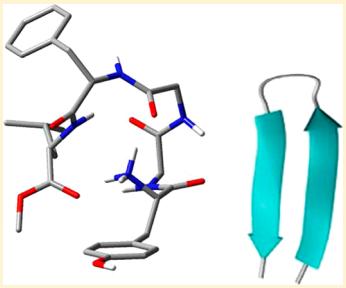

1. INTRODUCTION

The preferred structures taken up by peptides and proteins rest on a delicate balance of intramolecular and intermolecular interactions that control their folding, binding, precipitation, and aggregation, often based on subtle changes in conditions. It is often difficult to ascertain what factors control these structural changes, presenting a monumental challenge to first-principles theoretical descriptions. In such circumstances, there is a need for incisive experimental tests that isolate certain important structure-determining factors. One fruitful avenue being pursued is studies of prototypical peptides in the gas-phase, where solvent effects are removed, and the connections with theory are most easily and directly made.

Structural studies of neutral gas-phase peptides have been carried out on expansion-cooled molecules, where infrared (IR) and ultraviolet (UV) spectroscopy can be brought to bear, sometimes in double-resonance form, to obtain IR and UV spectra of single conformations that can be compared with the predictions from theory. Such studies have discovered and spectroscopically characterized several emergent, prototypical secondary structures in neutral α-peptides, including mixed helices,[1] β-turns,[2,3] β-strands,[4] β-sheets,[4−6] and β-hairpins.[7,8]

In widening the scope of such gas-phase studies, the fundamental role played by charge in determining peptide structure stands as a large and important issue that is only recently being explored by spectroscopic interrogation.[9−17] One of the motivations for such work arises from the ongoing discussions in modern mass spectrometry regarding the degree to which the solution-phase three-dimensional structures of peptides and proteins remain intact during the electrospray ionization (ESI) process that brings the ions into the gas-phase.[18]

Two limiting-case viewpoints exist on how the excess proton from positive-mode ESI is accommodated in the biomolecular scaffold. On the one hand, the presence of a bare protonated site is undoubtedly a major electrostatic perturbation that might be anticipated to disrupt the peptide structure in a fundamental way as the peptide backbone reorients nearby C═O groups to bind to the protonated site. On the other hand, common peptide secondary structural elements are held together by networks of H-bonds that could be robust even to these charge-related perturbations. Furthermore, the charge sites themselves might nucleate secondary structure formation, as they are known to do for lysine-terminated peptides that form α-helices.[9−11,19,20]

In order to better test these viewpoints, detailed structural data are needed on an array of peptide and protein ions in the gas-phase. While mass spectrometry is an invaluable tool for determining the primary amino acid sequence via tandem mass spectrometry, determination of the three-dimensional structures of the gas-phase peptide or protein ions requires further

Received: January 5, 2016
Published: February 7, 2016

DOI: 10.1021/jacs.6b00093
J. Am. Chem. Soc. 2016, 138, 2849−2857

characterization tools. There has been a recent explosion of interest in gas-phase ion spectroscopy, fueled by the development of powerful laser-based methods for probing gas-phase ion structures. In recent years, the combination of gas-phase IR spectroscopy and high-level theoretical predictions has been demonstrated as a powerful method for determining the intrinsic structures of peptide ions. A variety of such methods, including wavelength dependent IR multiphoton dissociation (IRMPD),[21−26] "messenger spectroscopy" where the ion of interest is "tagged" with messenger atoms/molecules that are lost following IR absorption,[27−32] helium nanodroplet spectroscopy,[33,34] and IR-UV double-resonance techniques,[9−17] have been developed.

By cryogenically cooling ions prior to spectroscopic interrogation, the spectral complexity associated with the number of conformational isomers, hot bands, and sequence bands is reduced by collapsing the population down to the zero-point vibrational levels of the low energy conformers present in the mass spectrometer. The resulting decrease in spectral complexity facilitates the direct comparison of the experimental spectra with theoretical calculations, often leading to more precise spectral assignments than those made on the basis of room temperature data alone.[17] This IR-UV double-resonance approach is analogous to that used for the elucidation of conformational differences between neutral peptide structures[1,35,36] and has been recently demonstrated as a useful technique in the study of peptide ion structures.[9−11,13−17]

To elucidate the primary structure of a peptide or protein (i.e., the peptide or protein amino acid sequence), a variety of solution-phase derivatization methods can be employed to remove ambiguities in the fragmentation data. Derivatized peptides are also frequently used in studies aimed at understanding fragmentation mechanisms.[37−40] A common modification is the methyl esterification of the C-terminus and the carboxylic acids on the side chains of any aspartic acid and glutamic acid residues, resulting in a mass shift of 14 Da for each reactive site.[41,42] Methyl esterification allows for facile differentiation between *b* and *y* type fragment ions, while also providing a determination of the number of carboxylic acids sites in the peptide.

Despite their widespread use in tandem mass spectrometry experiments, relatively little research has focused on how the incorporation of these mass tags affects the overall conformational preferences of peptide ions. Here we present the application of IR-UV double-resonance spectroscopy in a cryogenically cooled 22-pole ion trap for the structural investigation of protonated, C-terminally methyl esterified leucine enkephalin, $[YGGFL\text{-}OMe+H]^+$. The biologically active endogenous opioid peptide leucine enkephalin has been extensively studied as a model peptide in mass spectrometry in its unmodified protonated form $[YGGFL+H]^+$.[43] The gas-phase fragmentation pathways of protonated leucine enkephalin (m/z = 556 Da) upon collision induced dissociation (CID) have been studied comprehensively, particularly with regard to the lowest energy fragmentation pathway, cleavage of the F−L amide bond to form the b_4 ion (m/z = 425).[44−47] Although the C-terminally methyl esterified form of leucine enkephalin has not received the same kind of attention as its protonated form, it is known that the dissociation of $[YGGFL\text{-}OMe+H]^+$ proceeds through the same fragmentation channels as $[YGGFL+H]^+$, with a 14 Da shift observed for the C-terminal fragment ions.[48] Additionally, fragmentation of methyl esterified leucine enkephalin requires approximately the same amount of energy as that of its unmodified form.[48] However, it is known that $[YGGFL\text{-}OMe+H]^+$ actually has a higher biological potency than its nonmodified form, as measured with the guinea pig ileum myenteric plexus-longitudinal muscle bioassay.[49]

The structures of protonated leucine enkephalin and its low energy fragments have been studied with a variety of methods, including ion mobility spectrometry (IMS)[47] and spectroscopy.[21,16,17] The first cold UV photofragment and IR-UV double-resonance spectra of intact protonated leucine enkephalin were recently published by our research group,[17] leading to a revised structural assignment for this prototypical protonated peptide ion relative to that previously reported in an IRMPD study.[21] The assigned structure contains a single backbone conformation under cryo-cooled conditions, held together with multiple hydrogen bonds to C═O groups that self-solvate the NH_3^+ site. Additionally, the carboxylic acid OH group is engaged in a very strong H-bond, in which the OH group is flipped from its more typical *cis* position to the *trans* orientation to form an unusually short H-bond (1.72 Å) that is cooperatively strengthened by the NH_3^+ H-bond to its C═O group. The resulting $NH_3^+ \rightarrow O{=}C{-}OH \rightarrow O{=}C(F)$ H-bonds link the hydrogen bonding activity of the COO−H group to the F−L peptide bond, the cleavage of which results in the formation of the prevalent, low-energy b_4 fragment ion.

The effects of the ammonium charge site on this cooperatively strengthened hydrogen bonding environment are investigated in the work recently published by Florez et al.[34] in which helium nanodroplet spectroscopy was performed on the complex formed between protonated leucine enkephalin and 18-crown-6. Indeed, the hydrogen bonds that are cooperatively strengthened by solvation of the charge-site in protonated leucine enkephalin were observed to undergo large shifts to higher frequency in the IR spectroscopy of the 18-crown-6 peptide complex due to the fact that 18-crown-6 preferentially coordinates protonated amine sites. Based on that work, it is unclear whether the disruption to the structure is attributable to the loss of electrostatic interactions of NH_3^+ with the peptide or to the size of the crown ether, which could necessitate restructuring of the peptide in response to binding.

As we shall see, the main conformer of $[YGGFL\text{-}OMe+H]^+$ has a peptide backbone structure that shares much in common with its underivatized parent $[YGGFL+H]^+$, despite removing the OH group responsible for the strongest H-bond in the latter ion. The combined results on $[YGGFL\text{-}OMe+H]^+$ and $[YGGFL+H]^+$ provide new perspective on the common structural elements shared by the two ions. As we shall see, the $[YGGFL+H]^+$ and $[YGGFL\text{-}OMe+H]^+$ ions share a common secondary structural motif for the peptide backbone, the β-hairpin, with the NH_3^+ group stabilizing this secondary structure rather than disrupting it.

2. EXPERIMENTAL SECTION

2.1. Spectroscopic Methods. All spectroscopic data were acquired on an instrument described previously (see Figure S1).[17,50] Briefly, ions are generated via nanoelectrospray ionization (nESI). After introduction into the vacuum system, the ions pass through a home-built ion funnel, a quadrupole ion deflector, and a quadrupole ion guide, q1, before being trapped in a linear ion trap (LIT), q2. While in q2, the parent ion of interest is isolated via a notched pulsed-chirped broadband waveform. The isolated parent ion is then turned by a second quadrupole ion deflector through two transport quadrupoles before entering a 22-pole ion trap held at 5 K by a closed cycle helium cryostat (Sumitomo Heavy Industries, Tokyo,

DOI: 10.1021/jacs.6b00093
J. Am. Chem. Soc. 2016, 138, 2849−2857

Japan). A pulse of ultrapure He (99.9999%) is introduced into the 22-pole ion trap 1−3 ms before the ions are introduced to facilitate the trapping and cooling of the ions.

To record laser-induced UV photofragmentation spectroscopy of the cryogenically cooled ions, a UV laser pulse from the frequency-doubled output of a pulsed tunable dye laser (either ScanMate Pro or ScanMate, Lambda Physik) pumped by the second harmonic of a Q-switched Nd:YAG laser (Brilliant B, Quantel; Surelite II-20, Continuum) overlaps the trapped ions on the axis of the 22-pole ion trap. The UV laser power was limited to ≤1.5 mJ/pulse using neutral density filters, and the focus of the beam (≈ 3 mm diameter) was adjusted to achieve an approximately linear response between photofragment signal and laser energy fluence.

Absorption of a UV photon promotes the parent ions to their first excited electronic state, which is at an energy above the dissociation threshold, resulting in fragmentation of some fraction of the ions. Any residual parent ions and any photofragments resulting from irradiation are transported back through the transport quadrupoles and the second quadrupole ion deflector to an additional LIT, q3. Here a broadband waveform calculated by SX Wave software[51] is applied by a waveform generator (33220A, Agilent Technologies) to eject any parent ions remaining after irradiation. At this point, only photofragment ions remain in q3, and they can be analyzed by either mass selective axial ejection (MSAE),[52] or they can be dumped as an ion packet onto the channeltron detector (4773G, Photonis USA) in a total photofragment mode. All spectroscopic data presented herein were collected in this total photofragment mode. As reported previously for protonated leucine enkephalin,[17] the primary UV photodissociation products that comprise the total photofragment signal of $[YGGFL\text{-}OMe+H]^+$ are loss of the tyrosine side-chain (107 Da) and the known low energy CID-type fragment (b_4, a_4, y_3, y_2/b_3) ions. As reported previously,[17,50] an overlapped scan function was developed that involves the simultaneous and independent trapping of ions in q2 and the cold trap/q3. This allows for an effective filling time for q2 of 60 ms, a q3 analysis ramp of 60 ms, and a cooling time of 25 ms in the 22-pole cold trap, all within a 100 ms time frame, which accommodates coupling with the 10 Hz repetition rate of the lasers.

To acquire conformation-specific vibrational spectra, the UV laser wavelength is fixed on one of the observed transitions in the electronic spectrum, and an IR pulse is spatially overlapped with and counter-propagating the UV laser, entering the 22-pole trap 100 ns before the UV laser pulse. As the IR frequency is tuned through the spectral region of interest, vibrational excitation of the parent ions prior to electronic excitation depopulates the ground state zero-point level, which is detected as a depletion in the abundance of the UV-induced photofragmentation products. The highly resolved electronic spectra allow for the detection of the depletion of only ions that contribute to the selected UV transitions, resulting in conformation-specific IR depletion spectra.

Alternatively, non-conformation-specific vibrational spectra can be recorded by fixing the UV laser wavelength to the red of the lowest energy electronic origin in the UV spectrum. Absorption of a resonant IR photon can lead to intramolecular vibrational energy redistribution (IVR) among accessible vibrational levels, resulting in statistically inhomogeneous broadening of the UV spectrum that produces broad absorption that extends to the red of the electronic origin. Because the UV laser is fixed to the red of any conformation-specific transitions, this method results in an IR gain spectrum that is an abundance-weighted composite of the spectra due to all conformers present. The IR spectroscopy reported here employs the tunable output of a seeded Nd:YAG (Surelite III-EX, Continuum, Santa Clara, CA) pumped optical parametric oscillator/optical parametric amplifier (OPO/OPA, LaserVision, Bellevue, WA). For generation of IR light in the amide I/II regions, an $AgGaSe_2$ crystal was fixed downfield of the OPO output. The laser wavelength scans for both lasers and the data acquisition are controlled via LabVIEW (LabVIEW 8.2, National Instruments). Each population of ions in the cold 22-pole ion trap is subjected to either a single UV laser shot or one IR laser shot and one UV laser shot.

2.2. Materials. Leucine enkephalin and acetyl chloride were purchased from Sigma−Aldrich (St. Louis, MO). Glacial acetic acid and methanol were purchased from Mallinckrodt (Phillipsburg, NJ). After methyl esterification, a stock peptide solution of 1.0 mg/mL was prepared in a 50:50:1 methanol:water:acetic acid solution. The stock solution was diluted approximately 2-fold to produce the nESI working solution. Pulled borosilicate glass capillaries (Sutter Instruments, Novato, CA) were filled with 10 μL of the working solution for nESI. Methyl esterification of the C-terminus of leucine enkephalin was performed using established procedures.[40] Briefly, methyl esterification was performed by adding 80 μL of acetyl chloride dropwise to 500 μL of cold, dry methanol, while stirring. After 5 min, ∼1.0 mg of peptide was dissolved in 200 μL of this solution. The reaction was then allowed to proceed for ∼8 h at room temperature, after which time the product was dried using a Centrivap Concentrator (Labconco) and reconstituted in 1 mL of water.

2.3. Computational Methods. Multiple conformational searches were performed on a variety of different starting structures with the MACROMODEL suite of programs to generate a set of structures.[53] The Amber* force field was used to find stable minima within a 50 kJ/mol window of the global minimum for each conformational search.[54] Additionally, the previously assigned backbone structure of protonated leucine enkephalin[17] was used to generate starting structures for $[YGGFL\text{-}OMe+H]^+$ by arranging the OMe group in both *cis* and *trans* configurations relative to the ester carbonyl. The low-energy outputs of the conformational searches (400 structures in total) were then optimized using density functional theory (DFT). After geometry optimization, harmonic frequency calculations were performed in the Gaussian09 program.[55] To account for dispersive interactions, Truhlar's hybrid density functional M05-2X was used with the 6-31+G(d) basis set.[56] For the geometry optimizations, a tight optimization convergence criterion was specified, and all of the calculations were run with an ultrafine grid. On the basis of accepted values,[57,58] hydride stretch, amide I, and amide II vibrational modes are scaled by 0.938, 0.955, and 0.945, respectively, to account for anharmonicity in the calculated harmonic vibrational modes These scaling factors bring the calculated fundamentals into best agreement with those observed in the experimental vibrational spectrum.

3. RESULTS

3.1. Ultraviolet Spectroscopy. As with protonated leucine enkephalin, its C-terminally methyl esterified analogue has two possible chromophores available for UV excitation, the aromatic rings on the tyrosine (Y) and phenylalanine (F) side chains. The UV spectrum taken in the spectral region of the phenolic tyrosine, Y, chromophore for protonated C-terminally methyl esterified leucine enkephalin is shown in Figure 1. There is a clear electronic origin at 35 600 cm^{-1}, which represents a blue shift compared to those of bare protonated tyrosine (35 081 cm^{-1}, 35 111 cm^{-1}, 35 186 cm^{-1},

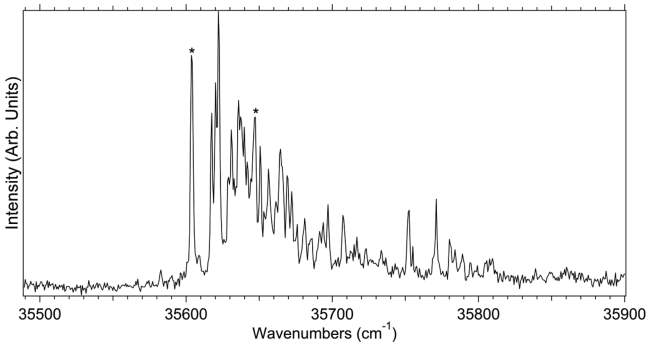

Figure 1. UV photofragment spectrum of $[YGGFL\text{-}OMe+H]^+$ in the region near the S_0-S_1 origin of the tyrosine chromophore with ∼1.5 mJ of UV laser power. The locations of the first and second electronic origins are marked with asterisks (*).

DOI: 10.1021/jacs.6b00093
J. Am. Chem. Soc. 2016, 138, 2849−2857

and 35 235 cm^{-1})[12,50] and a 84 cm^{-1} red shift compared to protonated leucine enkephalin (35 684 cm^{-1}).[17]

The UV spectrum has strong transitions present in the low energy portion of the spectrum and very dense vibronic structure that extends to higher wavenumbers. The two sharp transitions in the region between 35 740 and 35 775 cm^{-1} yield peak widths of full width at half-maximum (fwhm) of 3 cm^{-1}, indicating low rotational temperatures of 10 K or below. The spectrum for $[YGGFL\text{-}OMe+H]^+$ is compared with that for $[YGGFL+H]^+$ in the Supporting Information (Figure S2). Apart from the 84 cm^{-1} frequency shift, the spectra bear a remarkable resemblance to one another, suggesting that the tyrosine side chain is in a similar local environment in the two ions. Much of the observed low-frequency activity in the UV spectrum is attributable to Franck−Condon activity involving low-frequency vibrations associated with motion of the peptide backbone against the tyrosine ring. In many of the low energy conformations, the lowest frequency modes have frequencies near 10 cm^{-1}, comparable to the observed spacing in the spectrum in Figure 1. The rapid decay of intensity following the first two transitions reflects a relatively weak Franck−Condon progression, and as such a relatively minor geometry change between ground and excited states along these large-amplitude vibrational coordinates.

3.2. Infrared Spectroscopy. The IR-UV depletion spectra obtained in the amide I/II and the N−H stretch regions for $[YGGFL\text{-}OMe+H]^+$ with resonant UV excitation at 35 600 cm^{-1} are shown in Figures 2a and 2b, respectively.

The structure responsible for the stick spectra shown in Figure 2 is the global minimum among the 400 structures that were submitted to DFT optimization. In order to test for the presence of different conformers, IR depletion spectra were taken with the UV laser fixed on several of the strong vibronic bands in Figure 1, all of which were identical to those shown in Figure 2, indicating that there is one dominant conformer in the cold trap. However, non-conformation-specific IR gain spectra obtained in the amide I/II and N−H stretch regions indicate the presence of a second minor conformation by virtue of small additional transitions in the gain spectrum that do not overlap the main conformer IR absorptions, as shown in the Supporting Information (Figure S3).

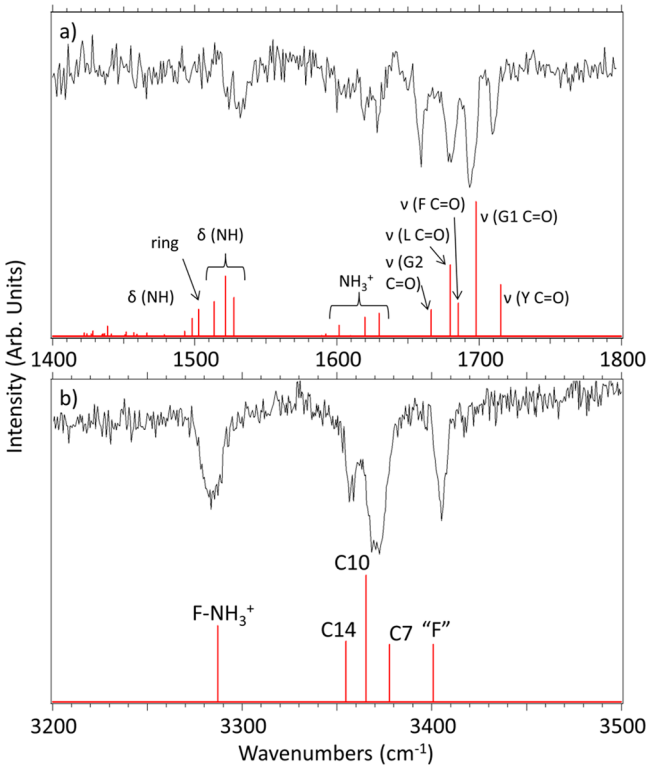

Figure 2. IR-UV photofragment depletion spectra for $[YGGFL\text{-}OMe+H]^+$ taken with resonant UV excitation at 35 600 cm^{-1} in the (a) amide I/II regions and (b) the N-H-stretch region. A table of the assigned vibrations is shown in the Supporting Information (Table S1).

Location of the second electronic origin due to this minor conformer was challenging due to dense vibronic activity to the blue of the first origin. Thus, IR-UV hole-burning was employed to find UV transitions corresponding to the minor conformer population. As shown in the Supporting Information (Figure S4), the strongest unique UV transition corresponding to the minor conformational isomer is located at 36 646 cm^{-1}, as marked with an asterisk in Figure 1. Conformation-specific IR depletion spectra obtained in the amide I/II and the N−H stretch regions with resonant UV excitation at 36 646 cm^{-1} are shown in the Supporting Information (Figures S5 and S6, Table S2). An unambiguous assignment for the structure of this minor conformer has not been possible to date, and so this conformer structure is not considered further in what follows.

4. DISCUSSION

4.1. Conformational Assignment. Figure 3 presents the structure assigned to the main conformer of $[YGGFL\text{-}OMe+H]^+$. The wavenumber positions and intensity patterns of the calculated and experimental transitions agree quite well after applying standard scaling factors, particularly in the amide N-H stretch and amide I regions. Two of the N-H stretch fundamentals involving the ammonium group are highly red-shifted, appearing in the 2900−3100 cm^{-1} region, and show substantial broadening, as shown in the Supporting Information (Figure S6). The calculations reproduce the correct frequency and intensity patterns for these transitions, but underestimate their frequency shift. This is consistent with previous reports on other peptide systems, where the π-bound and C=O bound N-H stretching fundamentals of the strongly H-bonded NH_3^+ group are broadened and the magnitude of their shift to lower frequency is underestimated by DFT.[15,17] Despite this, the excellent overall agreement between experiment and calculation enables a structural assignment to be made. In the IR spectrum, all of the amide N−H stretches are shifted significantly to lower frequency than the "free" position (3450−3500 cm^{-1}), indicating a strongly reinforced hydrogen bonding architecture. However, analysis of the DFT calculations indicates that the phenylalanine N-H stretch is nominally free despite its frequency shift, a phenomenon which was also observed for $[YGGFL+H]^+$ and will be described in greater detail in the following section.

In what follows, we use a Cn nomenclature common in the literature[35] that characterizes a H-bond by the number of atoms 'n' in the H-bonded ring that connects the hydrogen of the XH donor and the acceptor atom; N−H stretches that are not involved in a H-bond are designated as free (F). Using this nomenclature, the peptide backbone is designated from N-terminal to C-terminal $[NH_3^+(a)\_(b)\_(c)/$ NH(1)/NH(2)/NH(3)/NH(4)] as π_C17_C11/C14/C7/F/C10 (see Figure 3). The transitions involving the C7, C10, and C14 hydrogen bonded N−H stretches do not involve the ammonium group

DOI: 10.1021/jacs.6b00093
J. Am. Chem. Soc. 2016, 138, 2849−2857

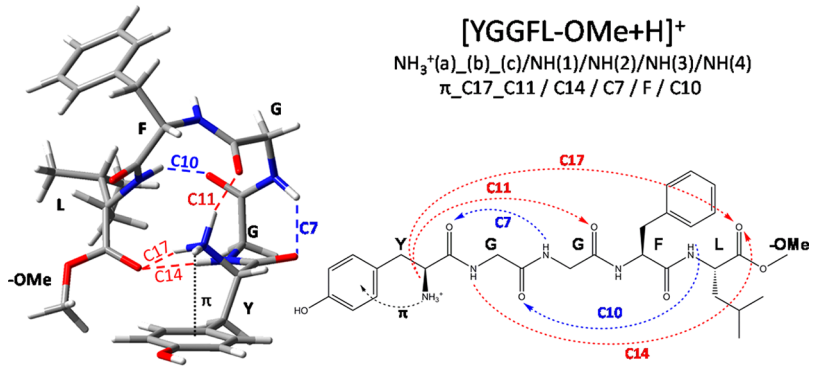

Figure 3. Labeled hydrogen bonding architecture of the dominant conformation (electronic origin at 35 600 cm^{-1}) of $[YGGFL\text{-}OMe+H]^+$. The red and blue dotted lines in the chemical structures link the groups connected by H-bonds, with donor−acceptor directions from N-terminal to C-terminal in red and from C- to N-terminal in blue.

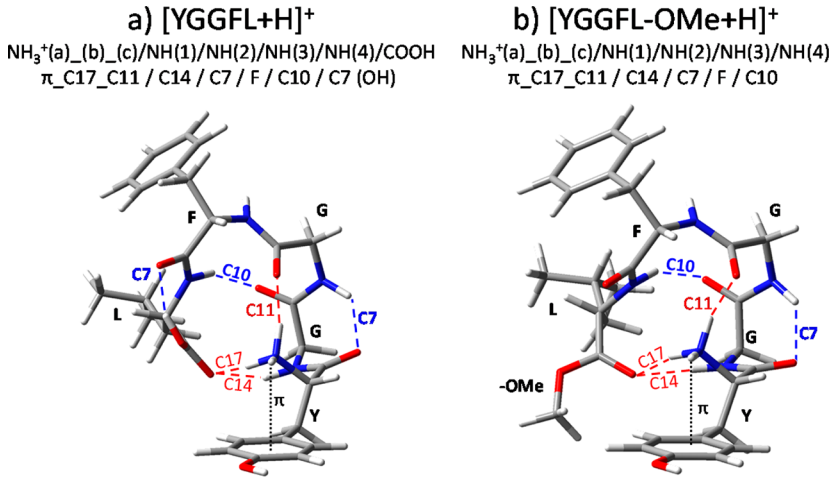

Figure 4. Comparison of the assigned structures for $[YGGFL+H]^+$ (a) and $[YGGFL\text{-}OMe+H]^+$ (b). For both structures the hydrogen bonding architecture is labeled. The red and blue dotted lines in the chemical structures link the groups connected by H-bonds, with donor−acceptor directions from N-terminal to C-terminal in red and from C- to N-terminal in blue.

directly and occur in the expected ranges previously observed for neutrals.[1,35,36] The transition involving the π-NH_3^+ H-bond is ∼50−75 cm^{-1} lower in frequency than that observed for a free N-H stretch of NH_3^+.[15] The methyl esterification of the C-terminus eliminates the COO-H transition from the spectrum.

The structure shown in Figure 3 is characterized by a backbone conformation held together by six H-bonds involving as donors all three NH_3^+ N-H groups and three of the four amide N-H groups. The presence of three hydrogen bonds to the ammonium group is in keeping with our expectation that, in the absence of solvent, the NH_3^+ charge site will engage in strong interactions with electron-rich regions of the peptide as the peptide self-solvates the charge. In $[YGGFL\text{-}OMe+H]^+$, the NH_3^+ group forms C11 and C17 H-bonded rings with the Gly^3 and C-terminus C═O groups, respectively, and a π H-bond with the tyrosine π-cloud. Amide-amide NH···O═C H-bonds account for the remainder. A C14 H-bonded ring ($i \rightarrow i+3$) is formed between the amide NH on the first glycine residue (Gly^2) and the same carbonyl oxygen of the C-terminus. A C10 H-bonded ring connects the amide NH on the leucine (Leu^5) residue to the carbonyl oxygen on Gly^2, an ($i+3 \rightarrow i$) H-bond. Finally, an ($i+2 \rightarrow i$) C7 ring is formed between the amide NH on the second glycine residue (Gly^3) and the carbonyl oxygen on the tyrosine (Tyr^1) residue.

Although 400 unique structures were analyzed via DFT, only three additional structures were found within 20 kJ/mol of the global minimum assigned here. These four low energy structures fall into two distinct families, with the assigned structure and its analogous structure with the OMe group in the *trans* configuration relative to the ester carbonyl constituting one family. The other two structures are characterized by a hydrogen bonding architecture given by F_C17_C11/C11/C7/C7/π following the Cn nomenclature. A more detailed comparison of these two conformational families, including their structures and predicted IR transitions, is given in the Supporting Information (Figures S7, S8, and S9).

4.2. Comparison to Protonated Leucine Enkephalin. The assigned structure for the dominant conformation of $[YGGFL\text{-}OMe+H]^+$ bears striking similarities to the structure previously assigned to its unmodified form.[17] A comparison of the assigned structures for $[YGGFL+H]^+$ and $[YGGFL\text{-}OMe+H]^+$ is shown in Figure 4.

It is clear from Figure 4 that $[YGGFL\text{-}OMe+H]^+$ and $[YGGFL+H]^+$ share the same hydrogen-bonding architecture, with the C14/C7/F/C10 peptide backbone structure identical, and the NH_3^+ group interacting with this peptide backbone in the same way, via π, C17, and C11 H-bonds. There are two principal differences between the two structures that are direct consequences of the substitution of methyl for hydrogen on the

DOI: 10.1021/jacs.6b00093
J. Am. Chem. Soc. 2016, 138, 2849−2857

C-terminus: (i) the methyl esterification modification eliminates the C7 hydrogen bond between the COO-H and the Phe[4] carbonyl oxygen, and (ii) the methyl group itself has reconfigured into a *cis* geometry from the *trans* geometry taken up by the OH group when it forms the C7 H-bond. Thus, while the C7 OH···O=C H-bond in $[YGGFL+H]^+$ is a very strong, short H-bond, evident in its large frequency shift and extreme broadening in the IR spectrum, the preferred structure of the ion is not determined by its presence, but instead is robust to its removal.

Table 1 summarizes the H-bond lengths of the shared H-bonds between the two ions, facilitating easy comparison.

Table 1. Hydrogen Bond Lengths for the Characteristic Backbone Hydrogen Bonds for $[YGGFL+H]^+$ and $[YGGFL-OMe+H]^+$

	hydrogen bond length (Å)	
assignment	$[YGGFL+H]^+$	$[YGGFL-OMe+H]^+$
C17	1.90	1.80
C11	1.84	1.74
C14	2.00	2.06
C7	2.11	2.15
C10	2.01	2.01
C7 (OH)	1.72	not applicable

While the C14, C10, and C7 peptide bonds are very similar in length, the H-bond lengths involving the NH_3^+ group (C17 and C11) are both ~0.1 Å shorter in $[YGGFL-OMe+H]^+$ than in $[YGGFL+H]^+$, pointing to the NH_3^+ group readjusting its position deeper into its binding pocket in response to the loss of the OH···O=C H-bond and reorientation to the *cis* configuration. Additionally, this is reflected by the further red-shifting of the calculated positions of the NH_3^+ stretches of $[YGGFL-OMe+H]^+$ by ~30 cm^{-1} (C17) and ~80 cm^{-1} (C11) relative to those of $[YGGFL+H]^+$.

The high level of structural similarity between the assigned structures for $[YGGFL+H]^+$ and $[YGGFL-OMe+H]^+$ is anticipated to result in close similarities in the UV and IR spectra of the two ions. As is shown in the Supporting Information (Figure S2), the UV spectra of $[YGGFL+H]^+$ and $[YGGFL-OMe+H]^+$ are relatively similar to one another, with the methyl ester's origin shifted only 84 cm^{-1} to the red of $[YGGFL+H]^+$, with both origins supporting similar Franck–Condon profiles involving low-frequency vibrations.

Figure 5 compares the IR spectra of $[YGGFL-OMe+H]^+$ (top) and $[YGGFL+H]^+$ (bottom) in the N-H stretch (right) and amide I (left) regions. Interestingly, while the IR spectrum for the dominant conformer of $[YGGFL-OMe+H]^+$ does show some resemblance to that for $[YGGFL+H]^+$, there are also significant differences that mask the structural similarities to some degree. In seeking an understanding of these differences, a deeper understanding of the spectroscopic consequences of close interaction of amide groups with the charge site can be gained.

In the N-H-stretch region, the C14, C7, and π NH_3^+ H-bonded transitions occur in roughly equivalent frequency positions in the two ions, consistent with the very similar H-bond lengths in Table 1. However, there are significant observed shifts in the frequencies of the C10 and free amide N-H stretches. In both $[YGGFL+H]^+$ and $[YGGFL-OMe+H]^+$, the nominally free phenylalanine N-H stretch is shifted down in frequency by almost 75 cm^{-1} from the typical frequency of a free amide N-H group (~3450 cm^{-1}) as a consequence of the protonated amine, which is H-bonded to this same amide group's C=O moiety via a C11 H-bond. As is seen in Figure 5, the free N-H stretch (F) for $[YGGFL-OMe+H]^+$ is also at an unusual frequency, and is shifted up in frequency by about 12 cm^{-1} compared to that of the parent $[YGGFL+H]^+$.

The most dramatic difference in the N-H stretch region occurs for the C10 H-bond between the Leu[5] amide NH and the Gly[2] carbonyl O, which is shifted to lower frequency by ~65 cm^{-1} in $[YGGFL+H]^+$ compared to $[YGGFL-OMe+H]^+$. This is completely at odds with the notion that H-bonded rings of the same size (e.g., C10) should appear in similar frequency regions, and prevented us early on from recognizing that the same C10 H-bond existed in both structures. Furthermore, the C10 H-bond is nearly identical in length in $[YGGFL+H]^+$ and $[YGGFL-OMe+H]^+$ (Table 1), indicating that the observed spectroscopic differences arise instead from electronic perturbations induced by the loss of the COO-H group in the methyl esterified peptide. In $[YGGFL+H]^+$, the Leu[5] amide NH C10 transition experiences an additional shift to lower frequency by virtue of the bare C-terminal COO-H, which is H-bonded to this same amide group's C=O moiety via an exceptionally strong (1.72 Å) C7 interaction. When this C7 interaction is eliminated by methyl esterification, the C10 H-bond occurs in the expected range previously observed for neutrals.[1,7,8,35,36] Thus, the C10 H-bond in $[YGGFL+H]^+$ is cooperatively strengthened by this backside C7 OH···O=C H-

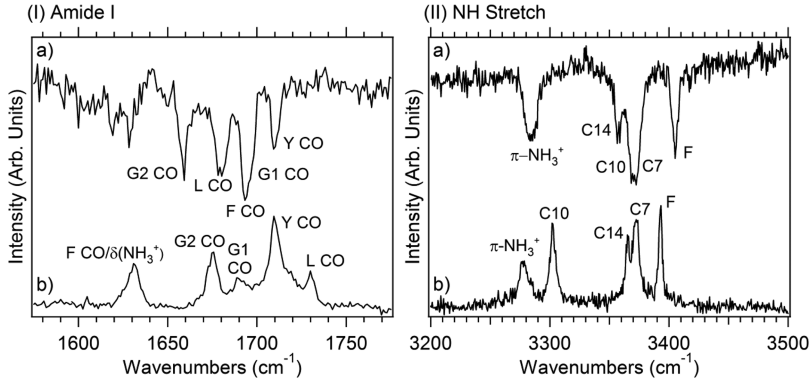

Figure 5. Comparison of the IR depletion spectra for $[YGGFL-OMe+H]^+$ (a) taken with resonant UV excitation at 35 600 cm^{-1} and the IR gain spectra for $[YGGFL+H]^+$ (b) taken with nonresonant UV excitation at 35 657 cm^{-1} in the amide I (I) and N-H-stretch (II) regions of the IR.

DOI: 10.1021/jacs.6b00093
J. Am. Chem. Soc. 2016, 138, 2849–2857

bond. It is noteworthy that the C7 H-bond completes a loop of cooperatively strengthened H-bonds:

$$\text{C-term OH(C7)} \rightarrow \text{O=C/NH(C10)} \rightarrow \text{O=C/NH(C7)} \rightarrow \text{O=C/NH(C14)} \rightarrow \text{O=C/OH}$$

that is broken in the absence of the C-terminal OH group in $[YGGFL\text{-}OMe+H]^+$.

Large differences are also seen in peak positions in the amide I region (Figure 5), most notably for the Leu^5 and Phe^4 carbonyl groups, with the former shifting down in frequency by 50 cm^{-1} upon esterification at this C-terminal site, and the Phe^4 C=O shifting up in frequency by a similar amount as the OH H-bond to C=O(F) is removed. The Gly^3 C=O also has its frequency lowered by a smaller amount (~15 cm^{-1}), consistent with the calculated shortening of the $NH_3^+\cdots$O=C(G) H-bond by 0.10 Å.

4.3. Effects of Charge on Secondary Structure: β-Hairpin Stabilization. Armed with the known structures for $[YGGFL+H]^+$ and $[YGGFL\text{-}OMe+H]^+$, we are now in a position to better assess the question posed in the introduction; namely, how does the presence of the protonated amine influence the preferred structures for the peptide backbone? Is it to be seen as a disrupter of secondary structure or are there circumstances in which the charge site enhances the stability of certain secondary structural motifs?

The side-by-side comparison of the observed structures for $[YGGFL+H]^+$ and $[YGGFL\text{-}OMe+H]^+$ in Figure 4 reveals the presence of a C14/C7/F/C10 sequence in the peptide backbone of both ions that is characteristic of a β-hairpin secondary structure,[59] the essential turn required for antiparallel β-sheet formation in longer peptide sequences. This β-hairpin is composed of (i) a nearest-neighbor C- to N-terminal C7 interaction between the Gly^3 amide NH and the Tyr^1 carbonyl O to form a γ turn, (ii) a C- to N-terminal C10 interaction between the Leu^5 amide NH and the Gly^2 carbonyl O that forms a type II′ β-turn, and (iii) an N- to C-terminal C14 H-bond between the Leu^5 and Gly^2 residues that completes the β-hairpin. In $[YGGFL+H]^+$, a second C7 H-bond between the COO-H and Phe^4 carbonyl O forms a γ_L turn (with the leucine side chain in an equatorial position relative to the C7 ring).

It is noteworthy that the β-hairpin secondary structure is energetically preferred over all alternatives by a rather wide margin (Figure S7), serving as the global minimum among computed structures in both ions. Furthermore, the β-hairpin retains this preferred status even when the strong OH···O=C C7 H-bond is lost by methyl esterification. Thus, $[YGGFL+H]^+$ and $[YGGFL\text{-}OMe+H]^+$ are examples in which a secondary structural motif, common to peptides and proteins *in vivo*, is preserved and even enhanced in stability by the presence of the unsolvated protonated amine charge site.

Figure 4 shows pictorially how the NH_3^+ site provides this additional stabilization. With minor perturbations to the network of H-bonds, C14/C7/F/C10(II′) and C14/C7/F/C10(II′)/C7L, that compose the β-hairpin, the NH_3^+ group sits in a binding pocket above the hairpin turn, forming a strong C11 H-bond to the Gly^3 carbonyl in an amide group not otherwise involved in the β-hairpin H-bonded network, at the center of the turn. Another of the NH_3^+ N-H groups forms a second stabilizing C17 H-bond with the C-terminal C=O, adding another connection between N- and C-terminus that draws together the ends of the hairpin.

As has already been pointed out, a comparison of the NH_3^+ binding pocket in $[YGGFL+H]^+$ and $[YGGFL\text{-}OMe+H]^+$ indicates that the C11 and C17 H-bonds involving the NH_3^+ group are shorter by ~0.10 Å, suggesting that the NH_3^+ group fits more snugly, and presumably more strongly, into the β-hairpin binding pocket in the methyl esterified derivative. It seems likely that this stronger binding is facilitated by the release of the *trans* OH···O=C H-bond present in $[YGGFL+H]^+$ and the structural relaxation that accompanies *cis* OCH_3 formation.

These C14/C7/F/C10(II′) and C14/C7/F/C10(II′)/C7L β-hairpin structures[59] have also been observed in isolated gas-phase neutral peptides by Mons and co-workers, where no NH_3^+ stabilization is present.[7,8] Here, we see that the intrinsic conformational preferences driving β-hairpin secondary structure formation extend to protonated ions. Prior to the present work, spectroscopic results reported for cold protonated peptides have focused on peptide sequences that form α-helices[9−11] or on the structural motifs present in a natively macrocylic peptide.[14] This work identifies the first evidence for β-hairpin formation in isolated gas-phase linear protonated peptides.

One intriguing aspect of these structural assignments in the gas-phase is that they are in agreement with the suggested bioactive form of the endogenous opioid peptide.[60−63] Leucine enkephalin is one of many opioid peptides that are known to bind to opioid receptors (μ, δ, κ) as a part of nervous and endocrine system regulation. The intrinsic flexibility afforded to leucine enkephalin in solution as a result of the inclusion of two adjacent glycine residues has complicated the assignment of its biologically relevant structure on the basis of traditional X-ray crystallography and NMR data alone.[64] The knowledge that opioid peptides are essentially disordered in aqueous media and that opioid receptors are membrane-bound proteins has led to the hypothesis that the peptide structure transitions from being disordered to more ordered and folded as it travels from the bulk aqueous environment into the water-membrane interface and finally into the apolar environment of the membrane lipids.[64] Studies of the structure of leucine enkephalin under an apolar environment indicate the presence of a type II′ β-turn around Gly^3-Phe^4 and a γ-turn around Gly^2,[60−63] which has been further supported by energy calculations.[65−67] Additionally, studies have shown that while biological activity is dependent upon inclusion of the N-terminal ammonium charge site, blocking of the C-terminal carboxylate charge site with a methyl esterification modification actually enhances biological activity.[49] These results indicate that the study presented herein of cryogenically cooled protonated leucine enkephalin and its C-terminally methyl esterified analogue in the gas-phase is an appropriate medium for studying the intrinsic conformational preferences of the peptide, and that the structures found in gas-phase studies may bear a closer resemblance to the low dielectric constant environment of biological membranes than to those preferred in aqueous solution.

5. CONCLUSIONS

The preferred conformation of cold, gas-phase protonated C-terminally methyl esterified leucine enkephalin was investigated in this work via UV and IR-UV double-resonance spectroscopy. A comparison of the IR spectra measured in the hydride stretch, amide I, and amide II regions to vibrational frequencies calculated via density functional theory indicates the presence of a backbone conformation analogous to that previously

DOI: 10.1021/jacs.6b00093
J. Am. Chem. Soc. 2016, 138, 2849−2857

assigned for the nonmodified peptide.[17] The assigned structures for $[YGGFL+H]^+$ and $[YGGFL\text{-}OMe+H]^+$ incorporate a C14/C7/F/C10(II′) H-bonded network characteristic of a β-hairpin peptide secondary structure. In this structure, the NH_3^+ charge site sits above the hairpin in a binding pocket that further stabilizes the β-hairpin, providing evidence that, in the right circumstance, the unsolvated charge site present in gas-phase ions can enhance rather than disrupt native protein secondary structures. The cryo-cooled gas-phase spectroscopy provides a unique window into the cooperative strengthening present in these H-bonded networks, and points the way for future studies aimed at characterizing other peptide sequences in which the charge site(s) either disrupt or enhance secondary structures common in natural environments.

■ ASSOCIATED CONTENT

Supporting Information

The Supporting Information is available free of charge on the ACS Publications website at DOI: 10.1021/jacs.6b00093.

A detailed schematic of the cold-ion spectroscopy instrument used in this work, a comparison of the UV spectra for $[YGGFL\text{-}OMe+H]^+$ and $[YGGFL+H]^+$, the assigned vibrational transitions for the dominant conformation, non-conformation-specific IR gain data, IR-UV hole-burning, IR depletion for the minor conformation, the vibrational transitions assigned to the minor conformation, and an analysis of the calculated low-energy structures for $[YGGFL\text{-}OMe+H]^+$ (PDF)

■ AUTHOR INFORMATION

Corresponding Authors

*mcluckey@purdue.edu

*zwier@purdue.edu

Present Addresses

†N.L.B.: Kellogg's, 2 Hamblin Avenue East, Battle Creek, MI 49017, United States.

‡J.G.R.: Kalsec, P.O. Box 50511, Kalamazoo, MI 49006, United States.

Notes

The authors declare no competing financial interest.

■ ACKNOWLEDGMENTS

Jim Zimmerman of the Jonathan Amy Facility for Chemical Instrumentation is acknowledged for his continued assistance in the design and operation of the instrument and associated electronics. Jim Hager and Frank Londry of AB Sciex are acknowledged for their helpful assistance with the SX Wave software. The authors gratefully acknowledge support from an NSF CRIF Instrumentation Development grant (CHE-0820766) for construction of the instrument, and NSF CHE-1213289 and CHE-1465028 (TSZ) and DOE FG02-00ER15105 (SAM) for operational and personnel costs.

■ REFERENCES

(1) Dean, J. C.; Buchanan, E. G.; Zwier, T. S. *J. Am. Chem. Soc.* **2012**, *134* (41), 17186−17201.

(2) Chin, W.; Compagnon, I.; Dognon, J. P.; Canuel, C.; Piuzzi, F.; Dimicoli, I.; von Helden, G.; Meijer, G.; Mons, M. *J. Am. Chem. Soc.* **2005**, *127* (5), 1388−1389.

(3) Chin, W.; Piuzzi, F.; Dimicoli, I.; Mons, M. *Phys. Chem. Chem. Phys.* **2006**, *8* (9), 1033−1048.

(4) Gerhards, M.; Unterberg, C. *Phys. Chem. Chem. Phys.* **2002**, *4* (10), 1760−1765.

(5) Fricke, H.; Gerlach, A.; Gerhards, M. *Phys. Chem. Chem. Phys.* **2006**, *8* (14), 1660−1662.

(6) Gerhards, M.; Unterberg, C.; Gerlach, A. *Phys. Chem. Chem. Phys.* **2002**, *4* (22), 5563−5565.

(7) Gloaguen, E.; Pollet, R.; Piuzzi, F.; Tardivel, B.; Mons, M. *Phys. Chem. Chem. Phys.* **2009**, *11* (48), 11385−11388.

(8) Plowright, R. J.; Gloaguen, E.; Mons, M. *ChemPhysChem* **2011**, *12* (10), 1889−1899.

(9) Stearns, J. A.; Seaiby, C.; Boyarkin, O. V.; Rizzo, T. R. *Phys. Chem. Chem. Phys.* **2009**, *11* (1), 125−132.

(10) Stearns, J. A.; Boyarkin, O. V.; Rizzo, T. R. *J. Am. Chem. Soc.* **2007**, *129* (45), 13820−13821.

(11) Stearns, J. A.; Boyarkin, O. V.; Rizzo, T. R. *Chimia* **2008**, *62* (4), 240−243.

(12) Stearns, J. A.; Mercier, S.; Seaiby, C.; Guidi, M.; Boyarkin, O. V.; Rizzo, T. R. *J. Am. Chem. Soc.* **2007**, *129* (38), 11814−11820.

(13) Stearns, J. A.; Guidi, M.; Boyarkin, O. V.; Rizzo, T. R. *J. Chem. Phys.* **2007**, *127* (15), 154322.

(14) Nagornova, N. S.; Guglielmi, M.; Doemer, M.; Tavernelli, I.; Rothlisberger, U.; Rizzo, T. R.; Boyarkin, O. V. *Angew. Chem., Int. Ed.* **2011**, *50* (23), 5383−5386.

(15) Wassermann, T. N.; Boyarkin, O. V.; Paizs, B.; Rizzo, T. R. *J. Am. Soc. Mass Spectrom.* **2012**, *23* (6), 1029−1045.

(16) Kopysov, V.; Nagornova, N. S.; Boyarkin, O. V. *J. Am. Chem. Soc.* **2014**, *136* (26), 9288−9291.

(17) Burke, N. L.; Redwine, J. G.; Dean, J. C.; McLuckey, S. A.; Zwier, T. S. *Int. J. Mass Spectrom.* **2015**, *378*, 196−205.

(18) Kalthashov, I. A.; Eyles, S. J. *Mass Spectrometry in Biophysics: Conformation and Dynamics of Biomolecules*; John Wiley & Sons: Hoboken, NJ, 2005.

(19) Hudgins, R. R.; Jarrold, M. F. *J. Am. Chem. Soc.* **1999**, *121* (14), 3494−3501.

(20) Kohtani, M.; Jones, T. C.; Schneider, J. E.; Jarrold, M. F. *J. Am. Chem. Soc.* **2004**, *126* (24), 7420−7421.

(21) Polfer, N. C.; Oomens, J.; Suhai, S.; Paizs, B. *J. Am. Chem. Soc.* **2007**, *129* (18), 5887−5897.

(22) Polfer, N. C.; Oomens, J.; Dunbar, R. C. *ChemPhysChem* **2008**, *9* (4), 579−589.

(23) Prell, J. S.; O'Brien, J. T.; Steill, J. D.; Oomens, J.; Williams, E. R. *J. Am. Chem. Soc.* **2009**, *131* (32), 11442−11449.

(24) Kupser, P.; Pagel, K.; Oomens, J.; Polfer, N.; Koksch, B.; Meijer, G.; von Helden, G. *J. Am. Chem. Soc.* **2010**, *132* (6), 2085−2093.

(25) Dunbar, R. C.; Steill, J. D.; Polfer, N. C.; Oomens, J. *J. Phys. Chem. A* **2013**, *117* (6), 1094−1101.

(26) Dunbar, R. C.; Oomens, J.; Berden, G.; Lau, J. K.-C.; Verkerk, U. H.; Hopkinson, A. C.; Siu, K. W. M. *J. Phys. Chem. A* **2013**, *117* (25), 5335−5343.

(27) Kamrath, M. Z.; Relph, R. A.; Guasco, T. L.; Leavitt, C. M.; Johnson, M. A. *Int. J. Mass Spectrom.* **2011**, *300* (2−3), 91−98.

(28) Kamrath, M. Z.; Garand, E.; Jordan, P. A.; Leavitt, C. M.; Wolk, A. B.; Van Stipdonk, M. J.; Miller, S. J.; Johnson, M. A. *J. Am. Chem. Soc.* **2011**, *133* (16), 6440−6448.

(29) Leavitt, C. M.; Wolk, A. B.; Kamrath, M. Z.; Garand, E.; Van Stipdonk, M. J.; Johnson, M. A. *J. Am. Soc. Mass Spectrom.* **2011**, *22* (11), 1941−1952.

(30) Leavitt, C. M.; Wolk, A. B.; Fournier, J. A.; Kamrath, M. Z.; Garand, E.; Van Stipdonk, M. J.; Johnson, M. A. *J. Phys. Chem. Lett.* **2012**, *3* (9), 1099−1105.

(31) DeBlase, A. F.; Kass, S. R.; Johnson, M. A. *Phys. Chem. Chem. Phys.* **2014**, *16* (10), 4569−4575.

(32) Marsh, B. M.; Voss, J. M.; Garand, E. *J. Chem. Phys.* **2015**, *143* (20), 204201.

(33) Filsinger, F.; Ahn, D.-S.; Meijer, G.; von Helden, G. *Phys. Chem. Chem. Phys.* **2012**, *14* (38), 13370−13377.

(34) Florez, A. I. G.; Ahn, D.-S.; Gewinner, S.; Schoellkopf, W.; von Helden, G. *Phys. Chem. Chem. Phys.* **2015**, *17* (34), 21902−21911.

DOI: 10.1021/jacs.6b00093
J. Am. Chem. Soc. 2016, 138, 2849−2857

(35) Kusaka, R.; Zhang, D.; Walsh, P. S.; Gord, J. R.; Fisher, B. F.; Gellman, S. H.; Zwier, T. S. *J. Phys. Chem. A* **2013**, *117* (42), 10847−10862.
(36) Gord, J. R.; Walsh, P. S.; Fisher, B. F.; Gellman, S. H.; Zwier, T. S. *J. Phys. Chem. B* **2014**, *118* (28), 8246−8256.
(37) Paizs, B.; Suhai, S. *Mass Spectrom. Rev.* **2005**, *24* (4), 508−548.
(38) Farrugia, J. M.; O'Hair, R. A. J.; Reid, G. E. *Int. J. Mass Spectrom.* **2001**, *210-211* (1−3), 71−87.
(39) Farrugia, J. M.; Taverner, T.; O'Hair, R. A. J. *Int. J. Mass Spectrom.* **2001**, *209* (2−3), 99−112.
(40) Reid, G. E.; Simpson, R. J.; O'Hair, R. A. J. *J. Am. Soc. Mass Spectrom.* **1998**, *9* (9), 945−956.
(41) Hunt, D. F.; Yates, J. R.; Shabanowitz, J.; Winston, S.; Hauer, C. R. *Proc. Natl. Acad. Sci. U. S. A.* **1986**, *83* (17), 6233−6237.
(42) Goodlett, D. R.; Keller, A.; Watts, J. D.; Newitt, R.; Yi, E. C.; Purvine, S.; Eng, J. K.; von Haller, P.; Aebersold, R.; Kolker, E. *Rapid Commun. Mass Spectrom.* **2001**, *15* (14), 1214−1221.
(43) Sztaray, J.; Memboeuf, A.; Drahos, L.; Vekey, K. *Mass Spectrom. Rev.* **2011**, *30* (2), 298−320.
(44) Asano, K. G.; Goeringer, D. E.; McLuckey, S. A. *Int. J. Mass Spectrom.* **1999**, *185-187*, 207−219.
(45) Goeringer, D. E.; Asano, K. G.; McLuckey, S. A. *Int. J. Mass Spectrom.* **1999**, *182-183*, 275−288.
(46) Laskin, J. *J. Phys. Chem. A* **2006**, *110* (27), 8554−8562.
(47) Polfer, N. C.; Bohrer, B. C.; Plasencia, M. D.; Paizs, B.; Clemmer, D. E. *J. Phys. Chem. A* **2008**, *112* (6), 1286−1293.
(48) Gaskell, S. J.; Reilly, M. H.; Porter, C. J. *Rapid Commun. Mass Spectrom.* **1988**, *2* (7), 142−5.
(49) Chavkin, C.; Goldstein, A. *Proc. Natl. Acad. Sci. U. S. A.* **1981**, *78* (10), 6543−6547.
(50) Redwine, J. G.; Davis, Z. A.; Burke, N. L.; Oglesbee, R. A.; McLuckey, S. A.; Zwier, T. S. *Int. J. Mass Spectrom.* **2013**, *348*, 9−14.
(51) Han, H.; Londry, F. A.; Erickson, D. E.; McLuckey, S. A. *Analyst* **2009**, *134* (4), 681−689.
(52) Londry, F. A.; Hager, J. W. *J. Am. Soc. Mass Spectrom.* **2003**, *14*, 1130−1147.
(53) Mohamadi, F.; Richards, N. G. J.; Guida, W. C.; Liskamp, R.; Lipton, M.; Caufield, C.; Chang, G.; Hendrickson, T.; Still, W. C. *J. Comput. Chem.* **1990**, *11* (4), 440−67.
(54) Weiner, P. K.; Kollman, P. A. *J. Comput. Chem.* **1981**, *2* (3), 287−303.
(55) Frisch, M. J.; Trucks, G. W.; Schlegel, H. B.; Scuseria, G. E.; Robb, M. A.; Cheeseman, J. R.; Scalmani, G.; Barone, V.; Mennucci, B.; Petersson, G. A.; Nakatsuji, H.; Caricato, M.; Li, X.; Hratchian, H. P.; Izmaylov, A. F.; Bloino, J.; Zheng, G.; Sonnenberg, J. L.; Hada, M.; Ehara, M.; Toyota, K.; Fukuda, R.; Hasegawa, J.; Ishida, M.; Nakajima, T.; Honda, Y.; Kitao, O.; Nakai, H.; Vreven, T.; Montgomery, J. A., Jr.; Peralta, J. E.; Ogliaro, F.; Bearpark, M.; Heyd, J. J.; Brothers, E.; Kudin, K. N.; Staroverov, V. N.; Kobayashi, R.; Normand, J.; Raghavachari, K.; Rendell, A.; Burant, J. C.; Iyengar, S. S.; Tomasi, J.; Cossi, M.; Rega, N.; Millam, J. M.; Klene, M.; Knox, J. E.; Cross, J. B.; Bakken, V.; Adamo, C.; Jaramillo, J.; Gomperts, R.; Stratmann, R. E.; Yazyev, O.; Austin, A. J.; Cammi, R.; Pomelli, C.; Ochterski, J. W.; Martin, R. L.; Morokuma, K.; Zakrzewski, V. G.; Voth, G. A.; Salvador, P.; Dannenberg, J. J.; Dapprich, S.; Daniels, A. D.; Farkas, Ö.; Foresman, J. B.; Ortiz, J. V.; Cioslowski, J.; Fox, D. J.*Gaussian 09*, Revision C.01, Gaussian, Inc., Wallingford CT, 2009.
(56) Zhao, Y.; Truhlar, D. G. *J. Chem. Theory Comput.* **2007**, *3* (1), 289−300.
(57) Buchanan, E. G.; James, W. H., III; Choi, S. H.; Guo, L.; Gellman, S. H.; Mueller, C. W.; Zwier, T. S. *J. Chem. Phys.* **2012**, *137* (9), 094301.
(58) Russell, D., Ed., *N.S.R.D.N. NIST Computational Chemistry Comparison and Benchmark Database*, Release 15a, Johnson III, April 2010,http://cccbdb.nist.gov/.
(59) Maynard, A. J.; Sharman, G. J.; Searle, M. S. *J. Am. Chem. Soc.* **1998**, *120* (9), 1996−2007.
(60) Deber, C. M.; Behnam, M. A. *Biopolymers* **1985**, *24*, 105−114.
(61) Milon, A.; Miyazawa, T.; Higashijima, T. *Biochemistry* **1990**, *29*, 65−75.
(62) Picone, D.; D'ursi, A.; Motta, A.; Tancredi, T.; Temussi, T. A. *Eur. J. Biochem.* **1990**, *192*, 433−439.
(63) Naito, A.; Nishimura, K. *Curr. Top. Med. Chem.* **2004**, *4*, 135−145.
(64) Spadaccini, R.; Temussi, P. A. *Cell. Mol. Life Sci.* **2001**, *58*, 1572−1582.
(65) Isogai, Y.; Nemethy, G.; Scheraga, H. A. *Proc. Natl. Acad. Sci. U. S. A.* **1977**, *74*, 414−418.
(66) Loew, G.; Keys, C.; Luke, B.; Polgar, W.; Toll, L. *Mol. Pharmacol.* **1986**, *29*, 546−553.
(67) Maigret, B.; Fournie-Zaluski, M. C.; Roques, B. P.; Premilat, S. *Mol. Pharmacol.* **1986**, *29*, 314−320.

DOI: 10.1021/jacs.6b00093
J. Am. Chem. Soc. 2016, 138, 2849−2857